Energy 176 (2019) 91–102

Contents lists available at ScienceDirect

Energy

journal homepage: www.elsevier.com/locate/energy

Feature parameter extraction and intelligent estimation of the State-of-Health of lithium-ion batteries

Yuanwang Deng [a, c], Hejie Ying [a], Jiaqiang E [a, c, *], Hao Zhu [a, c], Kexiang Wei [b], Jingwei Chen [a, c], Feng Zhang [a, c], Gaoliang Liao [a, c]

[a] College of Mechanical and Vehicle Engineering, Hunan University, Changsha, 410082, China
[b] Hunan Provincial Key Laboratory of Vehicle Power and Transmission System, Hunan Institute of Engineering, Xiangtan, 411104, China
[c] Institute of the New Energy and Energy-saving & Emission-reduction Technology, Hunan University, Changsha, 410082, China

ARTICLE INFO

Article history:
Received 15 January 2019
Received in revised form
15 March 2019
Accepted 29 March 2019
Available online 29 March 2019

Keywords:
Lithium-ion battery
State-of-Health
Least squares Support Vector Machine
Feature selection
Multi-working conditions

ABSTRACT

In order to provide an accurate State-Of-Health (SOH) estimation, a novel estimation method is proposed in this paper. In this work, some battery SOH relate features are selected theoretically, proved and then re-screened mathematically. These features can reflect the battery degeneration from different aspects. Also, a new training set design idea is proposed for Least Squares Support Vector Machine algorithm, thereby a model that is suitable for lithium-ion Battery SOH estimation under multi-working conditions can be built. Several lithium-ion battery degeneration testing datasets from National Aeronautics and Space Administration Ames Prognostics Center of Excellence are used to validate the proposed method. Results demonstrate both the superiority of the proposed method and its potential applicability as an effective SOH estimation method for embedded Battery Management System.

1. Introduction

With the rapid development of automobile industry, automobile exhaust pollution has aroused extensive attention [1,2], therefore, some great efforts have been made by researchers in reducing the exhaust pollution by using of new combustion technologies (stabilizing combustion systems [3], new combustor [4], laminar co-flow diffusion combustion [5] and mitigating self-excited combustion [6]), after-treatment technologies (diesel particulate filter [7], exhaust gas recirculation [8] and turbocharger [9]), engine's energy recovery systems [10,11], or environment friendly bio-fuel (biodiesel [12,13], acetone-butanol-ethanol [14] and butanol-gasoline blends [15]). The demand for crude from automobiles will continue to be one of the main growth points of the global crude consumption in the next 20 years, which is a great challenge for the energy demand [16,17] and environment issue [18,19]. To solve the exhaust pollution fundamentally, electric vehicles are receiving more and more attention in recent years [20].

At present, the lithium-ion batteries are the most widely used battery type in electric vehicles due to its high energy density, low self-discharge effect and long cycle life, etc [21]. However, these advantages also cause some potential threats even the Battery Management System (BMS) has been applied to control them, e,g. safety, uniformity and battery useful life, etc [22,23]. Among these problems, how to estimate the battery State-of-Health (SOH) accurately has been the main issue of the BMS, because an accurate estimation of battery SOH can provide a reference for BMS in planning the control strategies and effectively avoiding potential safety hazards caused by excessive battery use [24,25]. In practice, however, the inducement of the capacity degeneration of the lithium-ion battery is so complicated that it is caused by the superposition of multiple factors, and none of them can be studied in isolation from each other, so the estimation of lithium-ion battery SOH is still a problem [26].

To obtain an accurate estimation for SOH, many methods have been proposed by the researchers in recent years, which can be roughly divided into three categories, i e, mechanism based method, adaptive method and data-driven method. The mechanism based method carry out the battery SOH estimation by establishing electrochemical model of battery, for which a deep research in battery electrochemical mechanism is required [27,28].

The Kalman Filter (KF) [29–31] and the Particle Filter (PF)

* Corresponding author. College of Mechanical and Vehicle Engineering, Hunan University, Changsha, 410082, China.
E-mail address: ejiaqiang@hnu.edu.cn (J. E).

https://doi.org/10.1016/j.energy.2019.03.177
0360-5442/

[32–34] are the representative theories in adaptive method, and also have been widely used in battery SOH estimation. As battery is a nonlinear system, the improved KF algorithm is usually adopted. In Ref. [29], dual extended Kalman filter and an auto regressive exogenous model was employed to detect battery parameters change and to obtain the values of battery SOH. The Extended Kalman Filter based SOH estimation methods are also developed [30,31]. The PF is considered a powerful tool in solving nonlinear problems. In Ref. [32], a Gauss-Hermite PF is developed to update the parameters of battery capacity degradation model in real time and predict the SOH of batteries. Mejdoubi et al. [33] proposed a Rao-Blackwellization PF base method for battery capacity and resistance estimation, which have shown good accuracy. And it has also been adopted to solve the non-Gaussian battery pack model SOH estimation problem [34]. Although the adaptive methods can obtain accurate SOH estimation results, but the factors that affects the capacity degeneration are not well considered, as a result, more battery test data is needed to re-build the model when the batteries working condition changes, otherwise it can hardly obtain accurate SOH estimation results as before. What's more, the re-build process has also put forward a challenge for embedded BMS's computational ability.

The data-driven method has became a hot spot in battery SOH estimation research in recent years, because it does not require in-depth study of the battery mechanism, and generally can obtain higher accuracy than the adaptive methods [26].

The data-driven method mainly includes Artificial Neural Network (ANN) [35–37], Gaussian Process Regression (GPR) [38–40] and Support Vector Machine (SVM), etc. ANN method has been frequently utilized for battery SOH estimation [35]. In Ref. [36], a SOH estimation framework based on ANN using dynamic condition data as the inputs was proposed. Chaoui et al. [37] presented an application of dynamically driven recurrent neural networks in battery analysis, in which a nonlinear auto-regressive with exogenous inputs architecture is designed for both State-Of-Charge (SOC) and SOH estimation. Besides ANN method, GPR is popular in data-driven method recently. Yu [38] developed an effective multi-scale logic regression and GPR based SOH estimation method for SOH and remaining useful life prediction. In Refs. [39,40], some improvements were made in kernel function and inputs of the GPR method to obtain more accurate SOH estimation.

The Support Vector Machine (SVM) is considered to be one of the most effective and widely used data-driven methods, because it can effectively solve the problem with little samples, problems with nonlinear characteristics, or high-dimensional problems. Therefore, it is considered a good choice in estimating the battery SOH. For example, an integrate model combines the classification and regression attributes of SVM is proposed in Ref. [41], in which the classification model provides a gross estimation, and the regression is for battery RUL (Remaining Useful Life) prediction. And the support vector regression-particle filter approach was proposed for battery SOH and RUL estimation [42]. Wei et al. [43] established a support vector regression based battery SOH state-space model to simulate the battery aging mechanism, and then employed a particle filter to estimate the impedance degradation parameters in order to suppress the measurement noises of current and voltage. Sometimes, Least Squares Support Vector Machine (LSSVM) is chosen in pursuit of faster computing speed and more accurate estimation. An integrated use of parameter-selection-based ensemble learning and LSSVM for battery SOH estimation has been proposed in Ref. [44]. Qisong Wang et al. [45] compared the accuracy of LSSVM and SVM in estimating battery SOH, and demonstrated that the LSSVM is simpler and more accurate than that based on SVM. DuoYang et al. [46] proposed a LSSVM based SOH estimation method and had verified its accuracy and generalization ability compared to ANN based method. Besides the application in SOH estimation, LSSVM is also used to improve the prediction accuracy of battery SOC [47,48].

The data-driven researches mentioned above can obtain good estimation results under specific working conditions, but as we all know that the working conditions of electric vehicles have great difference due to different driving habits and driving areas, which lead to different working conditions for batteries like temperature, discharge rate and depth of discharge [49], etc. Previous studies try to solve this problem by retraining the model as the working condition changes, but it not only requires certain computing power of the platform and certain amount of prior data, but also time-consuming, which increased hardware and experimental costs. Consequently, the estimation of battery SOH under specific working conditions can hardly meet the actual needs.

To overcome the challenges in aforementioned studies, a LSSVM based method for accurate lithium-ion battery SOH estimation is proposed. The motivation is to realize credible online SOH estimation of the lithium-ion battery regardless the changes of discharging working conditions, while minimizing the later stage computing burden of the platform. First, to avoid the discharging uncertainty of batteries, input features of the proposed method are extracted from charging curves theoretically, proved and then re-screened mathematically. These features are not only readily available for the BMS on the market, but also more comprehensively reflect the battery degeneration phenomenon from aspects like capacity, internal resistance and charging performance changes. And then, a new training set design idea is proposed for LSSVM, it contains the battery data obtained from two different working conditions. In addition to the purpose of selecting LSSVM in Refs. [45–47], by employing the LSSVM, the characteristics of the training set can be fully integrated, so that a more universal SOH estimation model can be build. Finally, the feasibility and universality of the proposed method are systematically verified using the battery testing datasets from NASA Ames Prognostics Center of Excellence (PCoE) [50].

The rest of this paper is organized as follows. In section 2, based on the lithium-ion battery degeneration data from NASA datasets, features that reflect the battery capacity degeneration are analyzed and re-screened, and then the construction of training set is also introduced. Section 3 introduced the reason LSSVM is chosen and how the proposed method is implemented, and the validation and discussion of the proposed method are carried out and conclusions are drawn.

2. Feature parameter extraction of the State-of-Health of lithium-ion batteries

In this section, the definition of the SOH and battery experiment of NASA PCoE is introduced, and then the features that are relevant to battery SOH are analyzed. Finally, the training and testing datasets for the proposed method are selected.

2.1. Battery State-of-Health

SOH is a general term for the degree of battery degeneration, thus there are several different definitions about SOH, such as capacity ratio [31,35,38,39], RUL [41–43,48] and internal resistance [49], etc. Among them, capacity ratio is the most commonly used definition. So in this paper, we adopt the capacity ratio as the definition of the battery SOH, which is shown in Eq.(1), where the C_{now} represents the maximum allowable discharge capacity, C_0 represents the nominal capacity of the battery.

$$SOH = C_{now}/C_0 \quad (1)$$

2.2. Experimental data analysis

The NASA datasets were collected from a custom built battery prognostics test bed comprising commercial lithium-ion 18650 sized rechargeable batteries. In the experiments, batteries were run through 3 different operational profiles (charge, discharge and impedance) at specified ambient temperature. Charging was carried out in a Constant Current (CC) mode at 1.5A (i e. 0.75C) until the battery voltage reached 4.2 V, and then continued in a Constant Voltage (CV) mode until the charging current dropped to 20 mA. Discharging was carried out under different loads so as to study the battery degeneration phenomenon under different working conditions.

In this paper, 'Discharging - Charging' is considered as a cycle. And it should be noticed that some of data in the NASA datasets are bad data, for example, in the dataset of battery #5 (the battery numbers in this paper are corresponding to the number in NASA datasets) a charge cycle data between record 310 and 313 is missing, so this cycle data during simulation will be deleted. Similar situations exist in other battery datasets, which will be not specifically pointed out in the following works.

2.3. Theory-based feature value selection

The input features play a decisive role in the accuracy of data-driven methods [51], therefore, the features that are theoretically related to battery SOH are selected, and then proved, re-screened mathematically.

It is known that battery degeneration is mainly affected by its working temperature, voltage and current, and its degeneration degree is also reflected in the changes of these three characteristics. Thus, the main problem is when and how shall we take them. The working conditions of the battery can be roughly divided into to charging and discharging. Between these two conditions, discharging process is volatile as it is mostly depend on the drivers' habits, which make it difficult to extract stable and representative features from discharging process. On the contrary, as most charging strategy is based on the CC-CV strategy mentioned in section 2.2, the charging process is relatively stable, hence more stable and representative features can be extracted to create a more accurate SOH estimation model.

Eddahech et al. [52], compared the degeneration data of lithium-ion batteries and concluded that the charging time in CC charging phase decreases with the degeneration degree, also pointed out that the performance of batteries can not be completely determined by CC charging process. Yang et al. [53], observed the current curve in CV charging phase of lithium batteries in different degeneration degrees, and concluded that as the degeneration degree of the battery is deepened, the changing rate of the current in the CV charging phase is gradually slowed down, which result in a gradual increase in the charging time in CV phase.

The shortening of CC charging time indicates the deepening of battery polarization, and the increasing of CV charging time indicates the weakening of lithium intercalation ability [54]. Both of these are caused by the decay of lithium battery materials actually, so they reflect the battery degeneration to a certain extent. Based on that, we can speculate that the charging capacity of lithium batteries in the two charging phases may also have some changes in different battery degeneration degrees, e.g, the charging capacity in CC phase decreases gradually, while the charging capacity in CV phase increases gradually.

To prove these inferences, take battery #5 that were tested under typical experimental condition (CC-CV charging mode, 24°Cambient temperature, 2A discharging load, 2.7 V end of discharging voltage) to analyse the effects of battery degeneration on these features. As shown in Fig. 1, Fig. 1(a) and (b) are the charging voltage and current curves of battery #5 in the 30th, 60th, 90th, 120th, and 150th testing cycles. These voltage and current curves have shown the same laws as concluded [52,53]. The charging capacity trend of CC and CV charging phase under different battery degeneration degrees in Fig. 1(c) and (d) shown that the charging capacity in CC phase decreases gradually, while the charging capacity in CV phase increases gradually, which have confirmed the speculation that there is a certain correlation between the changes of these two indicators and battery degeneration.

Based on the conclusions and inferences above, 4 SOH relate features can be extracted from the charging process of the lithium-ion battery (detail settings of these features are shown in Appendix A.):

F1_tmp: The time interval of an equal charging voltage difference, which represents the CC charging time trend of lithium-ion batteries in different SOH.
F2_tmp: Charging capacity in CC phase, which represents the CC charging performance of lithium-ion batteries is in different SOH.
F3_tmp: The time interval of an equal charging current difference, which represents the CV charging time trend of lithium-ion batteries in different SOH.
F4_tmp: Charging capacity in CC phase, which represents the CV charging performance of lithium-ion batteries are in different SOH.

In addition to the features mentioned above, battery temperature is also an important indicator of its degeneration. Generally speaking, battery temperature change is mainly caused by internal heat generation due to electrochemical reactions and Joules effect heating known as I^2R heating (I=current and R=internal resistance) [55], among which, electrochemical reaction heat is called reversible heat, and Joules effect heat is called irreversible heat. Both of the electrochemical reaction rate and internal resistance are considered to be important indicators of battery deterioration. However, they are very difficult to get effective measurement in the practical application of lithium-ion batteries, so temperature is the only key parameter that can be grasped. Ye et al. [56] pointed out that reversible heat is dominant in low current discharge process and irreversible heat is dominant in high current discharge process. As the exothermic behavior of reversible heat during discharge corresponds to endothermic during charging, irreversible heat is exothermic both in charge and discharge process. Some speculations can be drawn as follows:

(1) The CC charging phase is dominated by irreversible heat, while the CV charging phase is reversible heat dominated.
(2) There is no clear boundary between reversible heat and irreversible heat during charging.

Still take battery #5 as example, Fig. 2(a) shows the temperature change of battery #5 in the 10, 20, …, 140, 150 testing cycles. It can be seen that the temperature drops in the beginning of the CC phase, and then rise up until the end of CC phase, and finally stable at ambient temperature in CV phase. In some of the cycles, there is a temperature rise at the end of the CV phase, it is caused by errors of testing instruments which lead to discharging behavior, as show in Fig. 2(b). As ambient temperature is stable during the test, the

temperature drop in the beginning of the CC phase is obviously due to the dominance of reversible endotherm caused by high initial reactant concentration. Similarly, the temperature rise is caused by irreversible exothermic, and the temperature drop in the CV phase is the result of a combination of heat dissipation, electrochemical reaction endothermic and irreversible exothermic reduction. Therefore, the speculations should be corrected as follows: the CC charging phase is mainly dominated by irreversible heat, while CV charging phase is co-dominant.

The discussions above have revealed the possible correlation between battery temperature and its electrochemical reaction rate and internal resistance of battery degeneration. Therefore, another 2 SOH relate features can be extracted from the charging process of the lithium-ion battery based on the inferences (detail settings of these features are shown in Appendix A.):

F5_tmp: The temperature changing rate of an equal charging voltage difference, which represents the comprehensive performance of irreversible heat in the CC charging phase when lithium-ion batteries is in different SOH, unit °C/h.

F6_tmp: The average temperature of an equal charging current difference, which represents the comprehensive performance of reversible heat and irreversible heat in the CV charging phase when lithium-ion batteries is in different SOH.

2.4. Relevance validation based on GRA theory

The Grey Relational Analysis is developed from the theory of grey systems and tries to measure the relational grade according to the similarity grade between factors. Thus, the grey correlation analysis provides a quantitative measure of a system development, and is very suitable for dynamic process analysis. The main steps are as follows:

a. Specify reference sequence $X_0 = \{x_0(i)\ |i = 1, 2, \ldots, n\}$ and comparison sequence $X_m = \{x_m(i)|i = 1, 2, \ldots, n\}$.
b. Data normalization.
c. Compute the correlation coefficient between each point in the comparison sequence X_m and the corresponding point in the reference sequence X_0. a is identification coefficient, $a \in (0,1)$, a is 0.5 in this paper.

$$\xi_m(i) = \frac{\min_m \min_i |x_0(i) - x_m(i)| + \alpha \max_m \max_i |x_0(i) - x_m(i)|}{|x_0(i) - x_m(i)| + \alpha \max_m \max_i |x_0(i) - x_m(i)|} \quad (1)$$

d. Computation of grey relational grade between comparison sequence X_m and reference sequence X_0.

$$r_m = \frac{1}{n} \sum_{i=1}^{n} \xi_m(i) \quad (2)$$

Take battery #5 as an example, Fig. 3 shows the tendency of 6 features mentioned in Section 2.3. It can be observed that feature F1_tmp, F2_tmp, F3_tmp and F4_tmp have clear trend, while feature F4_tmp and F5_tmp does not seem to have any laws. So, to further confirm the relevance between these features and battery SOH, the GRA method has been applied.

Table 1 shows the relational grades of these 6 features. The value closer to 1 indicates the greater relational grade. The relational grades of F5_tmp is relatively low compare to other 5 features, indicates that it can not fully represent battery degeneration. And, for the purpose of reducing the hardware burden of embedded BMS and reduce the dimension of the inputs, features are re-screened based on the GRA analyzing results. Finally 3 features are selected as the inputs of the proposed method. They are:

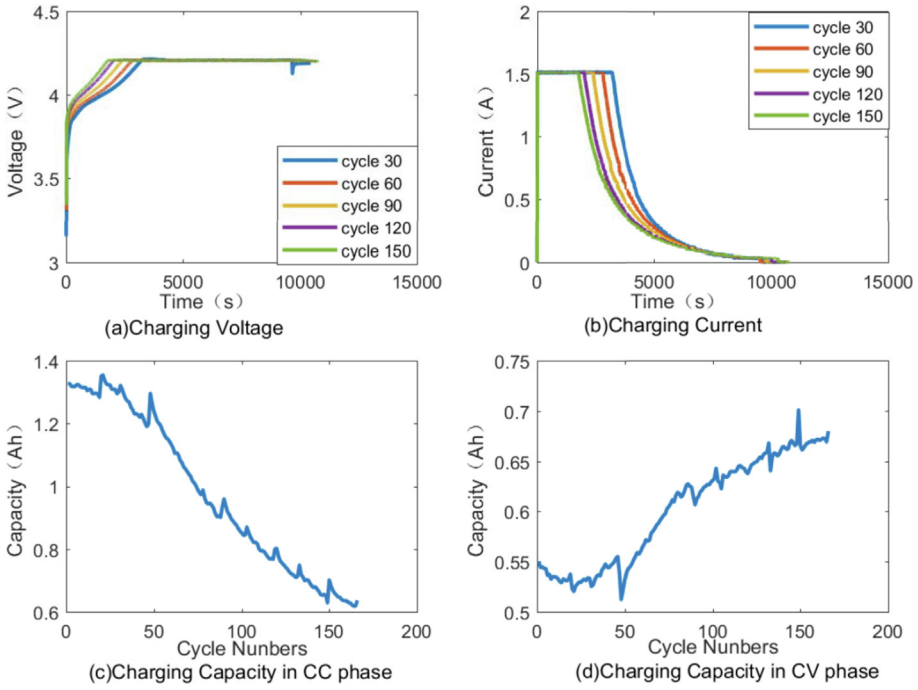

Fig. 1. Effects of battery degeneration on some features.

F1 The time interval of an equal charging voltage difference. Settings are consistent with F1_tmp.
F2 Charging capacity in CC phase. Settings are consistent with F4_tmp.
F3 The average temperature of an equal charging current difference. Settings are consistent with F6_tmp.

Also, considering that the battery SOH gradually decays as the cycle increases. So the SOH value estimated in the previous cycle is adopted as a feature at this time, so as to keep the SOH estimation results in a range.

F4 The SOH value estimated last time. Considering that initial battery SOH is usually unknown, so we unified the initial SOH to 0.9 in this paper, i.e, $F4\,(1) = 0.9$.

2.5. Selection of training and testing data

In addition to the battery #5 used in the above section, other 7 battery datasets from NASA datasets are selected, including battery #28, #31, #32, #38, #43, #44 and #56. Experimental conditions of these batteries are shown in Table 2, condition 1 means the battery is discharging under 0.05 Hz square wave loading profile of 4A amplitude and 50% duty cycle, condition 2 means the battery is discharging under multiple fixed load current levels (4A and 1A), condition 3 means the battery is discharging under multiple load current levels (1, 2, and 4 A).

Among them, the features extracted from battery #31 and #43 testing dataset are the training data for the proposed method, the features extracted from the rest of the batteries are treated as the testing data to validate the proposed method. The reason why we specially design the training set as a combination of battery #31 and #43 is to make the training set can represent an "interval working conditions", and then the LSSVM algorithm can be used to fuse the characteristics of the training set, so as to build a model that is suitable for battery SOH prediction under multi-working conditions. This is also the main reason for the selection of LSSVM algorithm in this paper, and why LSSVM can realize the fusion of training sets is determined by its mathematical theory. It will be introduced in Section 3.1.

It is worth mentioning that the discharging load of battery #31 and #43 is different, this may lead to the differences in their degeneration mechanism, but lead to the same result, i e, degeneration of battery SOH, and this will finally reflect on the changes of selected features. Also, the proposed method intends to explore the battery SOH estimation strategy from data-driven perspective rather than mechanism, and the chosen features are extracted from the same CC-CV charging process, the difference in discharging load will not affect the rationality of the conclusion of the proposed method.

3. Intelligent estimation of the State-of-Health of lithium-ion batteries

In this section, a brief view of the theory of SVM and LSSVM is provided including why LSSVM is chosen. And then the LSSVM based SOH estimation method is introduced. Finally, the proposed method is validated and discussed using NASA datasets.

3.1. Support Vector Machine and least squares Support Vector Machine

SVM was first proposed by Vapnik and applied to classification problems [57]. With the development and improvement of statistical theory, SVM is gradually applied to regression problems, and has shown great performance in the function approximation problems, especially the high-dimensional function approximation problems [58].

For linear regression problems, given a training set $\boldsymbol{T} = \{(x_i, y_i) | i = 1, 2, \ldots, n\}$, $x_i \in R^m$, $y_i \in R$, SVM find the best objective function $f(x) = w^T x + b$ by solving convex quadratic programming problem:

$$\min_{w,b,\xi,\xi^*} \quad \frac{1}{2}\|w\|^2 + C\sum_{i=1}^{n}\left(\xi_i + \xi_i^*\right),$$
$$s.t. \quad \begin{cases} ((w \cdot x_i) + b) - y_i \le \varepsilon + \xi_i, i = 1, \ldots\ldots, n \\ y_i - ((w \cdot x_i) + b) \le \varepsilon + \xi_i^*, i = 1, \ldots\ldots, n \\ \xi_i \ge 0, \xi_i^* \ge 0, i = 1, \ldots\ldots, n \end{cases} \tag{3}$$

where $C\,(C > 0)$ is the penalty parameter, represent the compromise between the flatness of the objective function $f(x)$ and the amount of deviation above the allowable ε. n means the size of the training set, ξ_i and ξ_i^* are slack variables.

In order to change the complexity of the problem and introduce the kernel trick, primal function and corresponding constraints in Eq. (3) are converted into dual problem by Lagrange Multiplier and KKT (Karush-Kuhn-Tucker) condition.

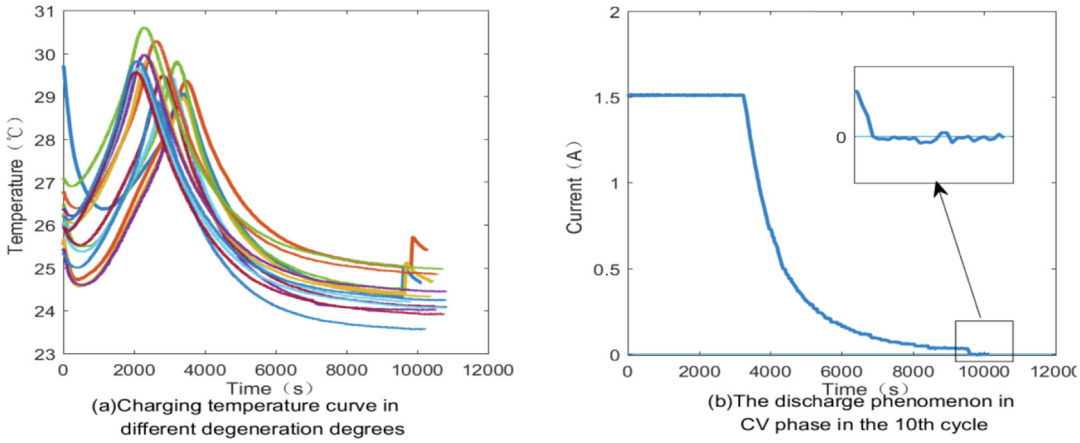

Fig. 2. Battery charging temperature curves under different degeneration degrees.

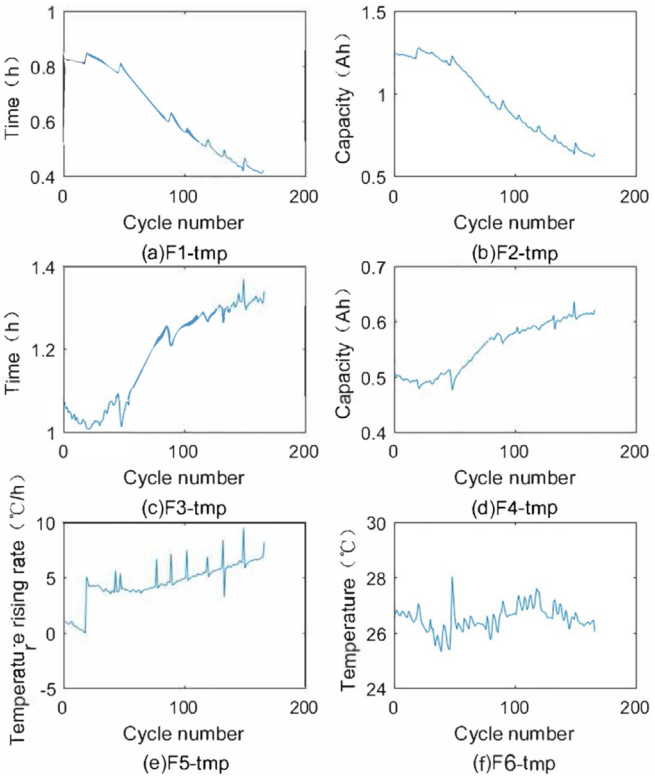

Fig. 3. Tendency of 6 extract features.

Table 1
GRA relational grades between features and battery SOH.

Features	Grey relational grade r_m
F1_tmp	0.9896
F2_tmp	0.9891
F3_tmp	0.6757
F4_tmp	0.6946
F5_tmp	0.5675
F6_tmp	0.8944

$$\min_{a_i^{(*)}} \frac{1}{2}\sum_{i,j=1}^{n}(a_i^*-a_i)\left(a_j^*-a_j\right)(x_i\cdot x_j)+\varepsilon\sum_{i=1}^{n}(a_i^*+a_i)-\sum_{i=1}^{n}y_i(a_i^*-a_i)$$
$$s.t.\begin{cases}\sum_{i=1}^{n}(a_i^*-a_i)=0\\ 0\le a_i^{(*)}\le C\ i=1,\ldots,n\end{cases} \tag{4}$$

where a_i, a_i^*, η_i and η_i^* are Lagrange multipliers, only the points that meet the condition $(a_i\text{-}a_i^*)\neq 0$ are support vectors (SVs). Now the objective function can be expressed as:

$$f(x)=\sum_{i=1}^{n}(a_i^*-a_i)(x_i\cdot x)+b \tag{5}$$

In order to generalize the SVM theory to nonlinear problems and simplify the calculation, kernel trick has been adopted. The resultant objective function is shown as follows:

$$f(x)=\sum_{i=1}^{n}(a_i^*-a_i)K(x_i,x)+b \tag{6}$$

where $K(x_i, x)$ is the kernel function, it has the forms of polynomial, linear and Radial Basis Kernel (RBF) functions, etc [59]. Among these kernel functions, the RBF kernel is one of the most popular choice, which can be represented as:

$$K(x_i,x)=\exp\left(-\gamma\|x_i-x\|^2\right) \tag{7}$$

where γ is the radius of the RBF kernel function.

As mentioned above, the objective function of SVM is determined only by a few SVs that meet the condition $(a_i - a_i^*)\neq 0$, which result in the sparseness of SVM. It is generally considered to be an advantage of SVM, because it simplifies the calculation while successfully avoiding dimensionality disasters. However it also bring about the dependence of the objective function on SVs, as a result, the objective function may not be able to characterize the training set because of some abnormal training points, or can only represent part of the characteristics of training set because the "misleading" of some training points. Therefore, in this paper, the LSSVM is employed to fully fuse the characteristics of the training set consists of two battery testing datasets.

LSSVM changes inequality constraints in SVM to equality constraints and estimate the error ξ by 2-norm (second-order norm), i e:

$$\min_{w,b,\xi}\ \frac{1}{2}\|w\|^2+\frac{C}{2}\sum_{i=1}^{n}\xi_i^2,$$
$$s.t.\quad y_i((w\cdot x_i)+b)=1-\xi_i, i=1,\ldots\ldots,n \tag{8}$$

For the same reason as SVM, primal function and corresponding constraints in Eq. (8) are converted into dual problem by Lagrange Multiplier and KKT (Karush-Kuhn-Tucker) condition.

$$\min_{a}\ \frac{1}{2}\sum_{i=1}^{n}\sum_{j=1}^{n}a_ia_j\left(K(x_i\cdot x_j)+\frac{\delta_{ij}}{C}\right)-\sum_{i=1}^{n}a_iy_i$$
$$s.t.\quad \sum_{i=1}^{n}a_i=0 \tag{9}$$

where a_i is Lagrange multipliers. The resultant optimized target function is expressed as follow:

$$f(x)=\sum_{i=1}^{n}a_iK(x_i,x)+b \tag{10}$$

As LSSVM replaces the ε-insensitive loss function used in standard SVM with quadratic loss function, all the training points in the training set are SVs to LSSVM, thus the objective function of LSSVM is able to fully fuse the characteristics of the training set. Therefore, with the proper design of the training set, LSSVM has competence to build a model that is suitable for battery SOH prediction under multi-working conditions.

It's also worth noticing that the training procedure of SVM has the time complexity about $O(n^3)$ [60], while is $O(n^2)$ for LSSVM (n is the number of training points). Both of their estimation complexity is $O(m)$ (m is the number of SVs). Generally speaking, LSSVM has more SVs than SVM, so it costs more time to finish the estimation. However, the proposed LSSVM based SOH estimation method don't need to the retrain the model as battery working condition changes, which actually saves a lot of time and reduce the computational burden.

Table 2
Experimental condition of selected batteries.

Battery	Temperature (°C)	Charging mode	Discharge current (A)	End of discharge (V)
#28	24	CC-CV	Condition 1	2.7
#31	43	CC-CV	4	2.5
#32	43	CC-CV	4	2.7
#38	24/44	CC-CV	Condition 3	2.2
#43	4	CC-CV	Condition 2	2.5
#44	4	CC-CV	Condition 2	2.7
#56	4	CC-CV	2	2.7

3.2. SOH estimation based on LSSVM

Based on the discussions above, the LSSVM based lithium-ion battery SOH estimation procedure is shown in Fig. 4. Firstly, corresponding testing datasets are obtained and features are extracted. Secondly, the training set is formed according to the proposed design idea and employed to optimize the kernel parameters (both SVM and LSSVM use RBF kernel function), and then build the LSSVM model as described in Section 3.1. Finally, the testing sets are applied to verify the accuracy and reliability of the proposed method, and its embedded time consumption test is also carried out.

3.3. Validation and discussion

Several tests based on the selected NASA datasets is performed to validate the proposed method. In addition, the selected features and the training set design idea are also applied to Back Propagation Neural Networks (BPNN) to further demonstrate their applicability to other data-driven methods. The results are shown and discussed in this section.

3.3.1. Evaluation criteria

According to the criteria adopted in Refs. [22,41], 3 evaluation criteria are employed to measure the estimation performance of proposed method.

(1) Root Mean Square Error (RMSE): to evaluate the deviation between the estimate SOH and real SOH.

$$RMSE = \sqrt{\frac{1}{n}\sum_{i=1}^{m}(SOH_{estimate} - SOH_{real})^2} \tag{11}$$

where n means the size of the dataset.

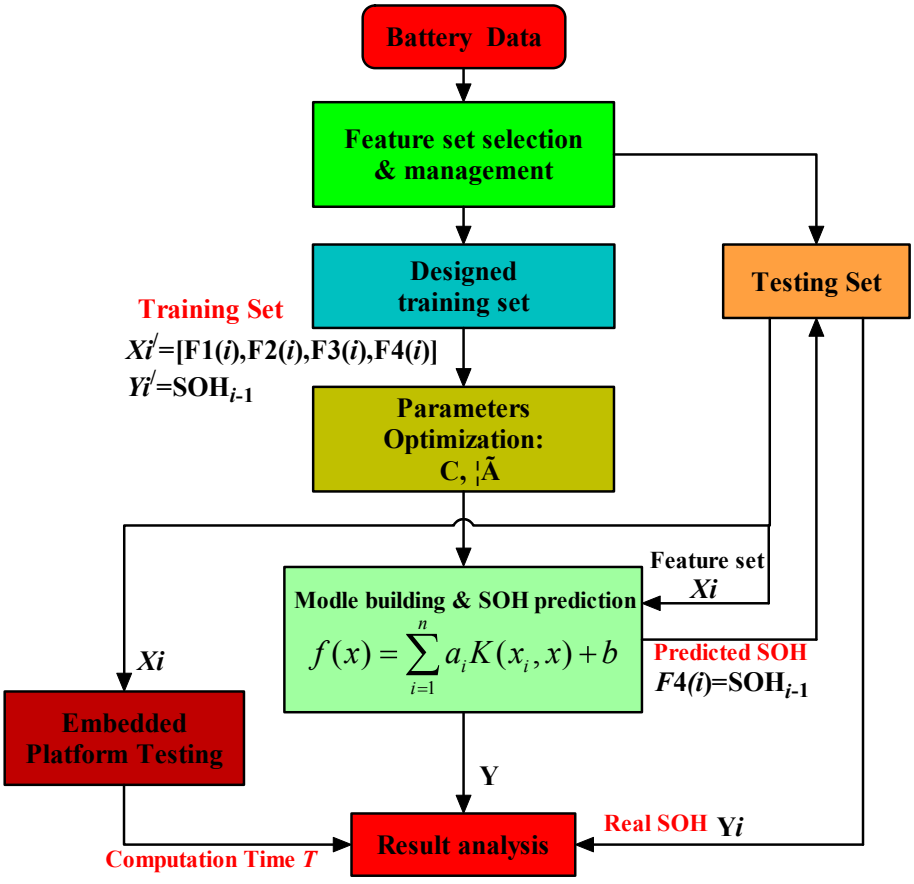

Fig. 4. SOH estimation process.

(2) SOH prediction errors: to show the estimation errors intuitively.

$$SOH_{errors} = |SOH_{estimate} - SOH_{real}| \tag{12}$$

(3) Coefficient of determination (R^2): to evaluate the degree to which the estimated values match the real values.

$$R^2 = 1 - \frac{\sum_{i=1}^{n} (SOH_{real}(i) - SOH_{estimate}(i))^2}{\sum_{i=1}^{n} (SOH_{real}(i) - SOH_{average}(i))^2} \tag{13}$$

3.3.2. Estimation results and discussion

As mentioned in section 2 that datasets of battery #5, #28, #32, #38, #44 and #56 are used to validate the proposed method. A comparison between standard SVM and LSSVM have been conducted, and the applicability verification of the selected features and the training set design idea is also carried out.

Fig. 5 shows the SOH estimation results and errors of battery #32, #44 and #28. It can be seen from Fig. 5(a) and (c) that the initial errors of proposed method are large, it is due to the initial value of *F*4 (1) that has been set to 0.9. In fact, the closer the *F*4 (1) to the real SOH initial value, the smaller the initial error will be, estimation result in Fig. 5(c) is an example. However, even if the initial *F*4 (1) leads to large errors, the proposed method can still stabilize the SOH estimation errors below 0.02 after several cycles, indicating the robustness of the proposed method. On the contrary, the errors of SVM based method is quite different for different batteries, which is caused by the "misleading" of SVs as mentioned in section 3.1. It can be deduced from Fig. 5 that most SVs of SVM based method are from battery #43, as its estimation performance is better on the battery tested under high temperature conditions. Overall the proposed method shows good short term estimation accuracy both in the same and different working conditions of the training set.

Features extracted from datasets of battery #5 and #56 are used to conduct the simulation to prove the long term estimation ability of proposed method. As shown in Fig. 6, the 89th cycle of battery #5 and the 48th cycle of battery #56 shows a large estimation error, in the same cycles, there are battery capacity regeneration phenomenons. As we do not fully consider the effect of this phenomenon, it causes certain estimation error in the corresponding cycles, which explains why the error curves of batteries #32, #5 and #56 are all broken lines, while battery# 44 has a smoother error curve. Besides that, SOH estimation errors of proposed method are almost under 0.02, demonstrate the ability of the proposed method in accurate long-term battery SOH estimation under the working conditions that is different from the training set.

Battery #38 was tested under condition 3 as mentioned in section 2.4, which is suitable for proving the estimation ability of proposed method under complex working conditions. As shown in Fig. 7, there is a catastrophe point in SOH estimation, which is corresponding to ambient temperature mutation point (24 deg C to 44 deg C) during the battery test. As mentioned in Ref. [61], the sudden change of temperature will lead to a significant change in battery performance, which leads to the failure of the extracted features to effectively characterize the battery system. This explain the catastrophe point and also reveal the shortcoming of the proposed method, i.e, drastic changes of ambient temperature in a discharge-charge cycle will result in terrible estimation performance. However, on the one hand, ambient temperature is usually relatively stable. On the other hand, to maintain the stability of battery temperature, BTMS (Battery Thermal Management Systems) using liquid [62] or air [61] as medium are equipped in most

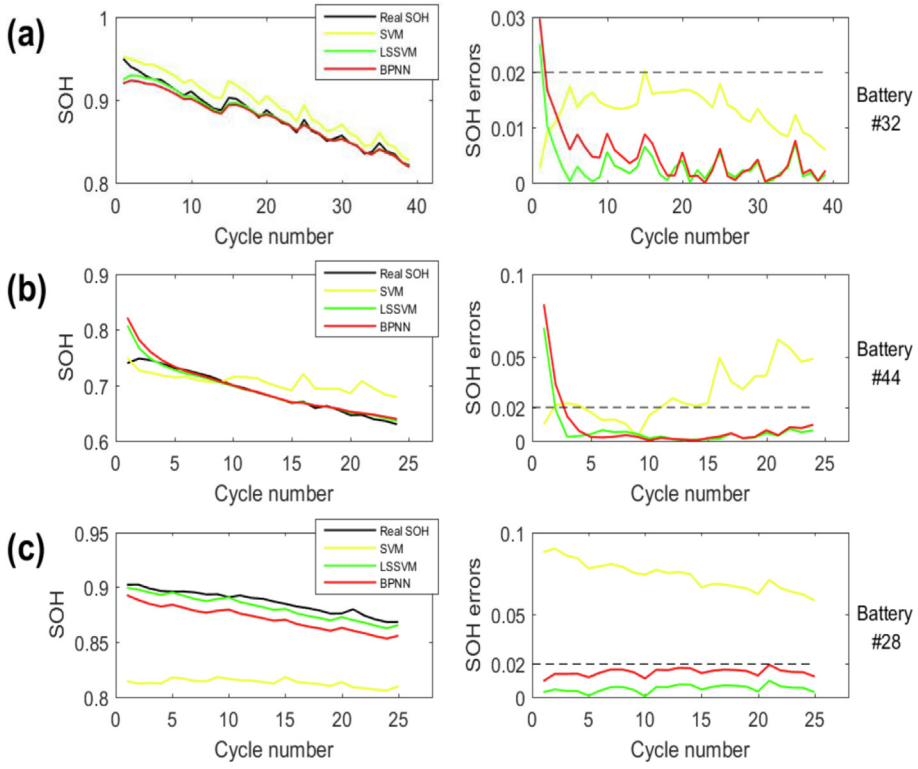

Fig. 5. SOH estimation results and errors of battery #44, #32 and #28.

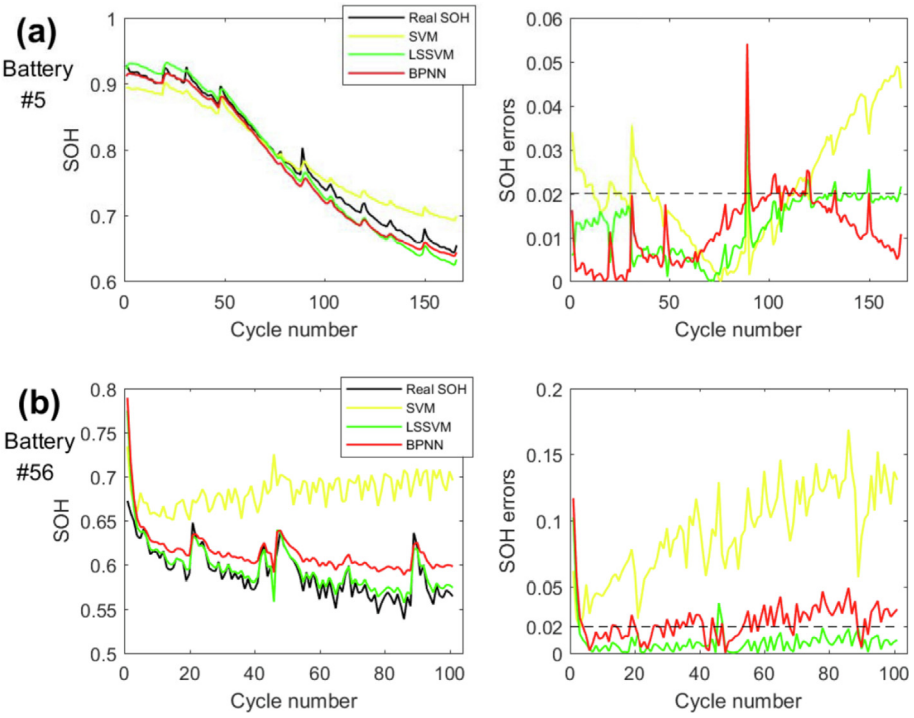

Fig. 6. SOH estimation results and errors of battery #5 and #56.

electric vehicles, researches show that with a proper designed BTMS, battery temperature change is slow and can be stabilized in a certain range [63,64]. Therefore, the shortcoming is tolerable in practical application. Despite of the catastrophe point, and the initial errors caused by improper *F*4 (1), the rest of the SOH errors are still under 0.02, shows that the proposed method has the ability to achieve accurate SOH estimation under complex working conditions.

In addition to the proposed LSSVM based method, BPNN based method is also tested in this section. It can be seen that the results of BPNN based method shown in Figs. 5–7 have shown similar characteristics to LSSVM based method. The selected features and the training set design idea are also applicable to other data-driven methods that have similar training data processing mode as LSSVM.

The RMSE and R^2 are employed to make a quantitative assessment of the estimation results. As shown in Table 3, the RMSEs of proposed LSSVM and BPNN based methods are fairly lower than SVM, and even lower than other methods proposed in Refs. [38,65], showing highly accuracy. The R^2 values of SVM based method is fluctuating or even negative, which means its model fits the battery system poorly. On the contrary, the R^2 values of LSSVM based method are all greater than 0.7, and BPNN based method are greater than 0.6, indicating that they have fit the battery system well.

Also, the proposed LSSVM based method is programmed to embed C language program, and tested on Freescale MC9S12XEP100 chip, which is one of the most widely used 16-bit chips. Results in Table 4 show that the proposed method cost about 30 ms to finish the calculation, satisfies the strict time requirement of embedded application.

In conclusion, based on the validations and discussions above, we can think that with the selected features, the proposed training set design idea, and a well-modeled LSSVM or some other data-driven methods that have similar training data processing mode as LSSVM, a universal model for accurate battery SOH online estimation under complex conditions can be built.

The proposed method is contrast to most previous studies on battery SOH estimation, which merely evaluate the accuracy of

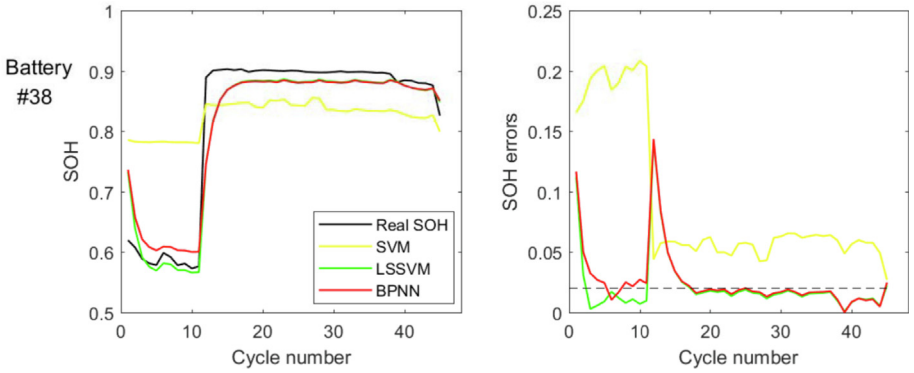

Fig. 7. SOH estimation results and errors of battery #38.

Table 3
RMSEs & R^2 of SOH estimation results by different methods.

Battery Number		#32	#44	#28	#5	#56	#38
RMSEs	SVM	0.0136	0.0317	0.0740	0.0247	0.0979	0.1077
	LSSVM	0.0053	0.0148	0.0055	0.0144	0.0144	0.0342
	ANN	0.0074	0.0188	0.0152	0.0135	0.0279	0.0367
R^2	SVM	0.8396	0.2812	−51.0362	0.9322	−12.4218	0.3329
	LSSVM	0.9758	0.8434	0.7083	0.9769	0.7115	0.9328
	ANN	0.9524	0.7488	0.6932	0.9798	0.6207	0.9223

Table 4
Time consumption test in embedded platform.

-	SVM	LSSVM
Time (ms)	5.179688	33.08594

proposed methods at a single arbitrarily selected cycle (e.g. treat the first half as training data, and rest is treated as testing data). To summarize, the proposed method has the advantage of high accuracy, robustness and universality, also has the potential applicability for embedded BMS. In addition, it's not only available for LSSVM, but also applicable to other data-driven methods that have similar training data processing mode as LSSVM.

However, in practice, different charging strategies may be applied to ensure the charging performance of batteries, thus some changes may be needed in feature selection rules of proposed method. Another limitation of proposed method is the effect of the size of the training set on computational load, which would directly affect the performance of the proposed method in embedded application. Therefore, in the next step, we will try to optimized the proposed method in the aspects of feature selection and data management (e.g., clustering analyse), so as to provide a more universal and faster SOH estimation method that is suitable for different kinds lithium batteries.

4. Conclusion

As for the more and more serious energy crisis [65–68] and emission issues [69–72] are accompanied by the economic development, the electric vehicles with its high energy density, low self-discharge effect and long cycle life can achieve a good balance between emission and energy with the restriction of more strict emission regulations. In this paper, a LSSVM based method for online lithium-ion battery SOH estimation under multi-working conditions is proposed and validated. The main contributions are summarized as follows:

(1) Some battery SOH relate features are selected theoretically, proved and re-screened mathematically from charging curves.
(2) A new training set design idea for LSSVM is proposed to build a more universal SOH estimation model for batteries under multi-working conditions.
(3) Several NASA datasets are adopted to verify the accuracy and robustness of proposed method, and the comparison with the standard SVM is also shown and discussed.
(4) Selected features and the training set design idea are also applied to BPNN to further demonstrate their applicability to other data-driven methods.
(5) The proposed method is tested on embedded platform to verify the feasibility of embedded application.

Conflicts of interest

The authors declare that they have no conflict of interests regarding the publication of this paper.

Acknowledgement

This work was supported by the Key Research and Development Projects of Hunan Science and Technology Plan [2017GK2201].

Appendix A. Features' settings

F1_tmp: The time interval of an equal charging voltage difference. In order to avoid the over-discharge in actual applications, usually avoid using the battery until the voltage drops below 3.0 V. Therefore, in this paper, the time interval of an equal charging voltage difference is the time when the battery voltage in the CC charging phase change from 3.5 V to 4.2 V.

F2_tmp: Charging capacity in CC phase. As the same consideration mentioned in F1_tmp, charging capacity in CC phase is the charging capacity when the battery voltage in the CC charging phase change from 3.5 V to 4.2 V.

F3_tmp: The time interval of an equal charging current difference. Considering that different charging strategies may be taken in CV charging phase in order to charge as much capacity as possible, the time interval of an equal charging current difference is the time from the beginning of CV charging phase until the current reaches 100 mA.

F4_tmp: Charging capacity in CC phase. As the same consideration mentioned in F3_tmp, charging capacity in CV phase is the capacity that charged from the beginning of CV charging phase until the current reaches 100 mA.

F5_tmp: The temperature changing rate of an equal charging voltage difference. As the same consideration mentioned in F1_tmp, equal voltage difference charging temperature rise rate is the average temperature changing rate when the battery voltage in the CC charging phase change from 3.5 V to 4.2 V.

F6_tmp: The average temperature of an equal charging current difference.As the same consideration mentioned in F3_tmp, the average temperature of an equal charging current difference is the average temperature from the beginning of CV charging phase until the current reaches 100 mA.

References

[1] E JQ, Zhao X, Xie L, Zhang B, Chen J, Zuo Q, Han D, Hu W, Zhang Z. Performance enhancement of microwave assisted regeneration in a wall-flow diesel particulate filter based on field synergy theory. Energy 2019;169:719–29.
[2] Deng Y, Zheng W, E JQ, Zhang B, Zhao X, Zuo Q, Zhang Z, Han D. Influence of geometric characteristics of a diesel particulate filter on its behavior in equilibrium state. Appl Therm Eng 2017;123:61–73.
[3] Zhao D, Lu Z, Zhao H, Li XY, Wang B, Liu P. A review of active control approaches in stabilizing combustion systems in aerospace industry. Prog Aero Sci 2018;97:35–60.
[4] Zhao D, Gutmark E, de Goey P. A review of cavity-based trapped vortex, ultra-compact, high-g, inter-turbine combustors. Prog Energy Combust Sci 2018;66:

42–82.
[5] Chu H, Han W, Cao W, Gu M, Xu G. Effect of methane addition to ethylene on the morphology and size distribution of soot in a laminar co-flow diffusion flame. Energy 2019;166:392–400.
[6] Wu G, Lu Z, Pan W, Guan Y, Li S, Ji CZ. Experimental demonstration of mitigating self-excited combustion oscillations using an electrical heater. Appl Energy 2019;239:331–42.
[7] E JQ, Zuo W, Gao J, Peng Q, Zhang Z, Hieu P. Effect analysis on pressure drop of the continuous regeneration-diesel particulate filter based on NO_2 assisted regeneration. Appl Therm Eng 2016;100:356–66.
[8] E JQ, Han D, Deng Y, Zuo W, Qian C, Wu G, Peng Q, Zhang Z. Performance enhancement of a baffle-cut heat exchanger of exhaust gas recirculation. Appl Therm Eng 2018;134:86–94.
[9] E JQ, Zhang Z, Tu Z, Zuo W, Hu W, Han D, Jin Y. Effect analysis on flow and boiling heat transfer performance of cooling water-jacket of bearing in the gasoline engine turbocharger. Appl Therm Eng 2018;130:754–66.
[10] Gabriel-Buenaventura A, Azzopardi B. Energy recovery systems for retrofitting in internal combustion engine vehicles: a review of techniques. Renew Sustain Energy Rev 2015;41:955–64.
[11] Zhao D, Li L. Effect of choked outlet on transient energy growth analysis of a thermoacoustic system. Appl Energy 2015;160:502–10.
[12] E JQ, Pham M, Zhao D, Deng Y, Le DH, Zuo W. Effect of different technologies on combustion and emissions of the diesel engine fueled with biodiesel: a review. Renew Sustain Energy Rev 2018;80:620–47.
[13] Zhang Z, E JQ, Chen J, Zhu H, Zhao X, Han D, Zuo W, Peng Q, Gong J, Yin Z. Effects of low-water addition on spray, combustion and emission characteristics of a medium speed diesel engine fueled with biodiesel fuel. Fuel 2019;239:245–62.
[14] Li Y, Tang W, Chen Y, Liu J, Lee CF. Potential of acetone-butanol-ethanol (ABE) as a biofuel. Fuel 2019;242:673–86.
[15] Zuo Q, Zhu X, Liu Z, Zhang J, Wu G, Li Y. Prediction of the performance and emissions of a spark ignition engine fueled with butanol-gasoline blends based on support vector regression. Environ Prog Sustain Energy 2019. https://doi.org/10.1002/ep.13042.
[16] Chen J, Xu W, Zuo H, Wu X, E JQ, Wang T, Zhang F, Lu N. System development and environmental performance analysis of a solar-driven supercritical water gasification pilot plant for hydrogen production using life cycle assessment approach. Energy Convers Manag 2019;184:60–73.
[17] Zhao X, E JQ, Wu G, Deng Y, Han D, Zhang B, Zhang Z. A review of studies using graphenes in energy conversion, energy storage and heat transfer development. Energy Convers Manag 2019;184:581–99.
[18] Chen J, Fan Y, E JQ, Cao W, Zhang F, Gong J, Liu G, Xu W. Effects analysis on the reaction kinetic characteristics of the food waste gasification by supercritical water. Fuel 2019;241:94–104.
[19] Wu G, Lu Z, Xu X, Pan W, Wu W, Li J, Ci J. Numerical investigation of aeroacoustics damping performance of a Helmholtz resonator: effects of geometry, grazing and bias flow. Aero Sci Technol 2019;86:191–203.
[20] E JQ, Yue M, Chen J, Zhu H, Deng Y, Zhu Y, Zhang F, Wen M, Zhang B, Kang S. Effects of the different air cooling strategies on cooling performance of a lithium-ion battery module with baffle. Appl Therm Eng 2018;144:231–41.
[21] Jiang Y, Jiang J, Zhang C, Zhang W, Li N. State of health estimation of second-life $LiFePO_4$ batteries for energy storage applications. J Clean Prod 2018;205:754–62.
[22] Sahinoglu GO, Pajovic M, Sahinoglu Z, Wang Y, Orlik P, Wada T. Battery state of charge estimation based on regular/recurrent Gaussian process regression. IEEE Trans Ind Electron 2018;65(5):4311–21.
[23] Lu L, Han X, Li J, Hua J, Ouyang M. A review on the key issues for lithium-ion battery management in electric vehicles. J Power Sources 2013;226(3):272–88.
[24] Nam W, Kim JY, Oh KY. The characterization of dynamic behavior of Li-ion battery packs for enhanced design and states identification. Energy Convers Manag 2018;162:264–75.
[25] Cheng Y, Lu C, Li T, Tao L. Residual lifetime prediction for lithium-ion battery based on functional principal component analysis and Bayesian approach. Energy 2015;90:1983–93.
[26] Berecibar M, Gandiaga I, Villarreal I, Omar N, Mierlo JV, Bossche PVD. Critical review of state of health estimation methods of li-ion batteries for real applications. Renew Sustain Energy Rev 2016;56(3):572–87.
[27] Baek KW, Hong ES, Cha SW. Capacity fade modeling of a lithium-ion battery for electric vehicles. Int J Automot Technol 2015;16(2):309–15.
[28] Zhang Q, White RE. Capacity fade analysis of a lithium ion cell. J Power Sources 2008;179(2):793–8.
[29] Tran NT, Khan A, ChoiW. State of charge and state of health estimation of AGM VRLA batteries by employing a dual extended kalman filter and an ARX model for online parameter estimation. Energies 2017;10(1). https://doi.org/10.3390/en10010137.
[30] Kim J, Cho BH. State-of-charge estimation and state-of-health prediction of a li-ion degraded battery based on an EKF combined with a per-unit system. IEEE Trans Veh Technol 2011;60(9):4249–60.
[31] Zou Y, Hu X, Ma H, Li SE. Combined state of charge and state of health estimation over lithium-ion battery cell cycle lifespan for electric vehicles. J Power Sources 2015;273:793–803.
[32] Schwunk S, Armbruster N, Straub S, Kehl J, Vetter M. Particle filter for state of charge and state of health estimation for lithium–iron phosphate batteries. J Power Sources 2013;239(10):705–10.
[33] Mejdoubi AE, Chaoui H, Gualous H, Bossche PVD, Mierlo JV. Lithium-ion batteries health prognosis considering aging conditions. IEEE Trans Power Electron 2018. https://doi.org/10.1109/TPEL.2018.2873247.
[34] Bi J, Zhang T, Yu H, Kang Y, Yan J. State-of-health estimation of lithium-ion battery packs in electric vehicles based on genetic resampling particle filter. Appl Energy 2016;182:558–68.
[35] Wu J, Wang Y, Zhang X, Chen Z. A novel state of health estimation method of li-ion battery using group method of data handling. J Power Sources 2016;327:457–64.
[36] You GW, Park S, Oh D. Real-time state-of-health estimation for electric vehicle batteries: a data-driven approach. Appl Energy 2016;176:92–103.
[37] Chaoui H. State of charge and state of health estimation for lithium batteries using recurrent neural networks. IEEE Trans Veh Technol 2017;66(10):8773–83.
[38] Yu J. State of health prediction of lithium-ion batteries: multiscale logic regression and Gaussian process regression ensemble. Reliab Eng Syst Saf 2018;174:82–95.
[39] Yang D, Zhang X, Pan R, Wang Y, Chen Z. A novel Gaussian process regression model for state-of-health estimation of lithium-ion battery using charging curve. J Power Sources 2018;384:387–95.
[40] Richardson RR, Osborne MA, Howey DA. Gaussian process regression for forecasting battery state of health. J Power Sources 2017;357:209–19.
[41] Nuhic A, Terzimehic T, Soczka-Guth T, Buchholz M, Dietmayer K. Health diagnosis and remaining useful life prognostics of lithium-ion batteries using data-driven methods. J Power Sources 2013;239:680–8.
[42] Dong H, Jin X, Lou Y, Wang C. Lithium-ion battery state of health monitoring and remaining useful life prediction based on support vector regression-particle filter. J Power Sources 2014;271:114–23.
[43] Wei J, Dong G, Chen Z. Remaining useful life prediction and state of health diagnosis for lithium-ion batteries using particle filter and support vector regression. IEEE Trans Ind Electron 2018;65(7):5634–43.
[44] Peng Y, Lu S, Xie W, Liu D, Liao H. Lithium-ion battery remaining useful life estimation based on ensemble learning with LS-SVM algorithm. Adv. Battery Manuf. Serv. Manag. Syst. 2016 https://doi.org/10.1002/9781119060741.ch9.
[45] Wang Q, Liu D, Zhang F, Zhang Y, Liu X, Wang H. Least squares support vector machine based lithium battery capacity prediction. In: International conference on mechatronics & control. IEEE; 2014. p. 1148–52.
[46] Yang D, Wang Y, Pan R, Chen R, Chen Z. State-of-health estimation for the lithium-ion battery based on support vector regression. Appl Energy 2018;227:273–83.
[47] Deng Z, Yang L, Cai Y, Deng H, Sun L. Online available capacity prediction and state of charge estimation based on advanced data-driven algorithms for lithium iron phosphate battery. Energy 2016;112:469–80.
[48] Meng J, Luo G, Gao F. Lithium polymer battery state-of-charge estimation based on adaptive unscented kalman filter and support vector machine. IEEE Trans Power Electron 2015;31(3):2226–38.
[49] Rezvanizaniani SM, Liu Z, Chen Y, Lee J. Review and recent advances in battery health monitoring and prognostics technologies for electric vehicle (EV) safety and mobility. J Power Sources 2014;256(12):110–24.
[50] Saha B, Goebel K. Battery data set, NASA ames prognostics data repository, moffett field, CA. 2007. http://ti.arc.nasa.gov/tech/dash/pcoe/prognosticdatarepository/.
[51] Pan H, Lü Z, Wang H, Wei H, Chen L. Novel battery state-of-health online estimation method using multiple health indicators and an extreme learning machine. Energy 2018;160:466–77.
[52] Eddahech A, Briat O, Vinassa JM. Determination of lithium-ion battery state-of-health based on constant-voltage charge phase. J Power Sources 2014;258:218–27.
[53] Yang J, Xia B, Huang W, Fu Y. Online state-of-health estimation for lithium-ion batteries using constant-voltage charging current analysis. Appl Energy 2018;212:1589–600.
[54] Wang Z, Zeng S, Guo J, Qin T. State of health estimation of lithium-ion batteries based on the constant voltage charging curve. Energy 2019;167:661–9.
[55] Pesaran AA. Battery thermal models for hybrid vehicle simulations. J Power Sources 2002;110(2):377–82.
[56] Ye Y, Shi Y, Cai N, Lee J, He X. Electro-thermal modeling and experimental validation for lithium ion battery. J Power Sources 2012;199:227–38.
[57] Cortes C, Vapnik V. Support-vector networks. Mach Learn 1995;20:273–97.
[58] E JQ, Qian C, Zhu H, Peng Q, Zuo W, Liu G. Parameter-identification investigations on the hysteretic Preisach model improved by the fuzzy least square support vector machine based on adaptive variable chaos immune algorithm. J Low Freq Noise Vib Act Control 2017;36(3):227–42.
[59] Wang A, Zhao Y, Hou Y, Yun-Lu L. A novel construction of SVM compound kernel function. Int. Conf. Logist. Syst. Intell. Manag. 2010;3:1462–5.
[60] Zheng S. A fast algorithm for training support vector regression via smoothed primal function minimization. Int. J. Mach. Learn. Cybern. 2015;6(1):155–66.
[61] Deng Y, Feng C, E JQ, Zhu H, Chen J, Wen M, Yin H. Effects of different coolants and cooling strategies on the cooling performance of the power lithium ion battery system: a review. Appl Therm Eng 2018;142:10–29.
[62] E JQ, Han D, Qiu A, Zhu H, Deng Y, Chen J, Zhao X, Zuo W, Wang H, Chen J, Peng Q. Orthogonal experimental design of liquid-cooling structure on the cooling effect of a liquid-cooled battery thermal management system. Appl Therm Eng 2018;132:508–20.
[63] E JQ, Xu S, Deng Y, Zuo W, Wang H, Chen J, Peng Q, Zhang Z. Investigation on thermal performance and pressure loss of the fluid cold-plate used in thermal

management system of the battery pack. Appl Therm Eng 2018;145:552–68.
[64] Qin T, Zeng S, Guo J. Robust prognostics for state of health estimation of lithium-ion batteries based on an improved PSO–SVR model. Microelectron Reliab 2015;55(9–10):1280–4.
[65] E JQ, Liu G, Liu T, Zhang Z, Zuo H, Hu W, Wei K. Harmonic response analysis of a large dish solar thermal power generation system with wind-induced vibration. Sol Energy 2019;181:116–29.
[66] Zuo H, Liu G, E JQ, Zuo W, Wei K, Hu W, Tan J, Zhong D. Catastrophic analysis on the stability of a large dish solar thermal power generation system with wind-induced vibration. Sol Energy 2019;183:40–9.
[67] E JQ, Jin Y, Deng Y, Zuo W, Zhao X, Han D, Peng Q, Zhang Z. Wetting models and working mechanisms of typical surfaces existing in nature and their application on superhydrophobic surfaces: a review. Adv. Mater. Interfac. 2018;5:1701052. https://doi.org/10.1002/admi.201701052.
[68] Xiong W, Wang Y, Mathiesen BV, Zhang X. Case study of the constraints and potential contributions regarding wind curtailment in Northeast China. Energy 2016;110:55–64.
[69] Wang H, Ou X, Zhang X. Mode, technology, energy consumption, and resulting CO_2 emissions in China's transport sector up to 2050. Energy Policy 2017;109:719–33.
[70] Deng Y, Cui J, E JQ, Zhang B, Zhao X, Zhang Z, Han D. Investigations on the temperature distribution of the diesel particulate filter in the thermal regeneration process and its field synergy analysis. Appl Therm Eng 2017;123:92–102.
[71] Zhang D, Karplus VJ, Cassisa C, Zhang X. Emissions trading in China: Progress and prospects. Energy Policy 2014;75:9–16.
[72] Ou X, Yan X, Zhang X. Life-cycle energy consumption and greenhouse gas emissions for electricity generation and supply in China. Appl Energy 2011;88(1):289–97.